Analysis of Magnetic Properties of Soft Magnetic Composite Using Magnetic Circuits Generated by Discrete Element Method

Hayaho Sato[1], Junichi Kotani[2], Yuma Sasaki[2], Shohei Tomioka[2], Toshiyuki Takizawa[2],

Yuki Ueda[2], Hirokazu Kimiya[2], Hajime Igarashi[1]

[1]Hokkaido University, Kita 9, Nishi 14, Kita-ku, Sapporo, 060-0814, Japan
[2]Panasonic Industry Co. Ltd., 1006, Kadoma, 571-8506, Japan

This paper proposes an effective method based on a magnetic circuit for the analysis of magnetic properties of soft magnetic composite (SMC). The present method constructs an imitation of SMC by the discrete element method (DEM), which analyzes the motion of the iron particles in SMC. Based on the resulting particle configuration, the magnetic circuit is generated, and the circuit equation is solved to evaluate the macroscopic permeability and the eddy current loss of the SMC assuming that the magnetic saturation is negligible. The microscopic material properties of the iron particles such as electrical conductivity and insulation layer thickness are identified so that the difference between the computed and measured macroscopic properties of SMC is minimal. The proposed method can effectively deal with thin insulation layers whose finite element modeling results in a huge number of elements. The computational cost for the proposed method is much lower than that of the finite element method. Furthermore, the computed macroscopic permeability and eddy current loss are shown to be consistent with the measured results with different filling rates.

Index Terms—**Discrete element method, eddy current loss, macroscopic permeability, magnetic circuit, soft magnetic composite.**

I. Introduction

SOFT MAGNETIC COMPOSITE (SMC), composed of a number of insulated iron particles, is widely used in a variety of electromagnetic devices such as inductors and electric motors. Various analysis methods have been proposed to analyze its properties. Ollendorff's formula [1] can be used for evaluating the macroscopic permeability of SMC. However, it has been pointed out that this method underestimates the macroscopic permeability especially when the filling rate is rather high, and the iron particles have different sizes [2], [3]. To analyze SMC with high filling rate, the unit cell method has been proposed [3], [4], [5]. In this approach, SMC is assumed to consist of unit cells, each of which includes an iron particle and surrounding non-magnetic material region. The macroscopic permeability and loss are evaluated by analyzing the electromagnetic field in the unit cell with finite element method (FEM). However, the accuracy degrades when the SMC particles have different sizes so that magnetic flux is concentrated along the paths with relatively low magnetic reluctance. To overcome this difficulty, a method based on the discrete element method (DEM) [7], [8] and FEM has been developed [3], [9], [10]. In this method, SMC is modeled by DEM where the motion of distributed particles is simulated. The properties of SMC are then evaluated using FEM where the FE mesh is generated for the particles resulted from DEM. Another method based on Voronoi tessellation has been proposed to obtain FE mesh of SMC that mimics the actual internal structure [11], [12]. It is also possible to convert the cross-sectional image of the magnetic core made of SMC into FE mesh [2]. Although these methods are effective, there is a difficulty that they are computationally expensive. This is due to the multi-scale nature of SMC. In general, the size of the SMC particles is up to hundreds of microns, whereas the thickness of the insulation layer on the particle surface is in the submicron range. This multi-scale nature of SMC makes the analysis of SMC computationally difficult, especially when the SMC model is three-dimensional. One remedy for this problem is the magnetic circuit method. Y. Ito *et al.* [2] have proposed the magnetic circuit method for the analysis of SMC properties where periodically arranged cubic particles are assumed for the structure of SMC. Since the insulation layer can be modeled as magnetic reluctances, fine meshing is not required in this method, and the computational cost is quite low compared to that of the FEM-based methods. However, the discrepancy of the computed macroscopic permeability from the measured one, due to the uniformity assumption, has been observed. In the same study, it has been suggested that this problem would be solved by considering the magnetic contact between particles.

In this paper, we propose a novel magnetic circuit method for the analysis of SMC properties. To account for the particle distribution of the SMC and the contact between particles through the insulating layer, we use DEM, which allows us to naturally model the configuration of iron particles. Then, the magnetic circuit is constructed based on the particle configuration resulted from DEM. The circuit equation is solved to evaluate the macroscopic permeability as well as the eddy current loss using the complex permeability [6], [13] introduced to the magnetic circuit. We identify the difficult-to-measure microscopic properties, such as the insulation layer thickness and electrical conductivity of the iron particles, so that the difference between the computed and measured macroscopic properties is minimal. Once the microscopic properties are identified, the macroscopic SMC properties can be evaluated using the proposed magnetic circuit for different

Manuscript received April 1, 2015; revised May 15, 2015 and June 1, 2015; accepted July 1, 2015. Date of publication July 10, 2015; date of current version July 31, 2015. Corresponding author: Hayaho Sato (e-mail: hayaho_sato@em.ist.hokudai.ac.jp).

Color versions of one or more of the figures in this paper are available online at http://ieeexplore.ieee.org.

Digital Object Identifier (inserted by IEEE).

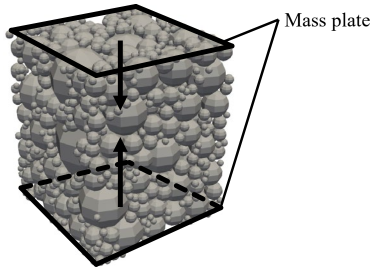

Fig. 1. Particles and mass plates in DEM.

TABLE I
SIMULATION SETTINGS IN DEM

Name	Value
Number of particles, N $(-)$	1182
Time step, Δt (s)	1.0×10^{-3}
Simulation time, t_{Max} (s)	1.0×10^{2}
Region dimensions	70 µm × 70 µm × 200 µm

particle distribution and filling rate.

II. MODELING OF SOFT MAGNETIC COMPOSITE

This section describes modeling of SMC based on DEM, which is used in the first step of the present method.

A. Discrete Element Method

DEM [7, 8] simulates the motion of spherical particles by solving the equation of motion given by

$$m_i \ddot{\boldsymbol{u}}_i = \sum_j \boldsymbol{f}_{ij} + \boldsymbol{F}_i, \tag{1a}$$

$$I_i \ddot{\boldsymbol{\theta}}_i = \sum_j \boldsymbol{T}_{ij}\,, \tag{1b}$$

where m_i, I_i, $\boldsymbol{u}_i$ and $\boldsymbol{\theta}_i$ denote mass, moment of inertia, displacement and rotational displacement of i-th particle, and $\boldsymbol{f}_{ij}, \boldsymbol{T}_{ij}$ denote the interacting force and rotational moment between i-th and j-th particles. The interactions $\boldsymbol{f}_{ij}, \boldsymbol{T}_{ij}$ are evaluated for the particles in contact, for which the criteria

$$D_{ij} \le r_i + r_j, \tag{2a}$$

$$D_{ij} = \|\boldsymbol{x}_i - \boldsymbol{x}_j\|, \tag{2b}$$

is used, where $r_i, r_j, \boldsymbol{x}_i, \boldsymbol{x}_j$ represent radius and center position of i-th (j-th) particle. In addition, we analyze the motion of the mass plates on which the external force $\boldsymbol{F}_i$ acts, which is described in section II. B.

B. Modeling of SMC

We consider iron particles in DEM for modeling of SMC, whose algorithm is summarized below [3], [9], [10]:

1. Generate radii of particles r_i $(i = 1, \ldots, N)$ from the given distribution of SMC particles.
2. Place N particles randomly in a three-dimensional region surrounded by walls.
3. Place mass plates above and below the particles. These mass plates are for mimicking the pressing process in manufacturing SMC.
4. Set simulation time $t \leftarrow 0$.

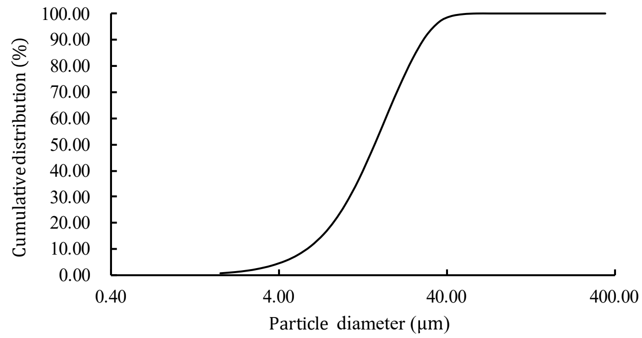

Fig. 2. Measured distribution of particles in SMC.

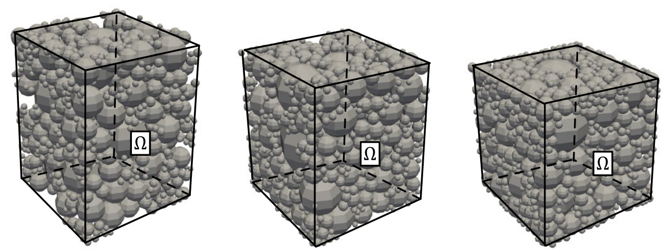

(a) model A1 (b) model A2 (c) model A3

Fig. 3. Final particles configurations obtained by DEM.

TABLE II
FILLING RATE OF SMC MODELS

Model name	Filling rate (%) (measured)	Filling rate (%) (DEM model, Fig. 3)
model A1	65.6	65.8
Model A2	73.8	73.0
Model A3	80.8	80.9

5. Solve equations (1a) and (1b) with time step Δt and the external force $\boldsymbol{F}_i$ for the mass plates to press the particles from top and bottom, as shown in Fig. 1.
6. Update the states of the particles and mass plates.
7. If t is greater than a given value t_{Max}, terminate process. Otherwise, set $t \leftarrow t + \Delta t$ and return to step 5.

The parameters for DEM is summarized in Table I. In this study, we generated r_i $(i = 1, \ldots, N)$ based on the measured distribution plotted in Fig. 2. We have three models A1, A2, and A3 which have the same size distribution but different filling rates. To generate these models, three DEM simulations were performed to adjust the filling rate by changing the mass of the plates while using the same particles.

Fig. 3 shows the final configuration of the particles in DEM. Hereafter, the regions Ω filled with the particles are treated as the SMC models. The contacts between the particles are detected based on the criteria (2a) and (2b) after completing the DEM simulation. Table II summarizes the filling rates of the three models, which are adjusted to the measured values. In section IV, model A2 is used to identify the microscopic parameters such as the insulation layer thickness and electrical conductivity of the iron particles, and models A1 and A3 are used to validate the identified parameters by comparing the measured and computed macroscopic properties.

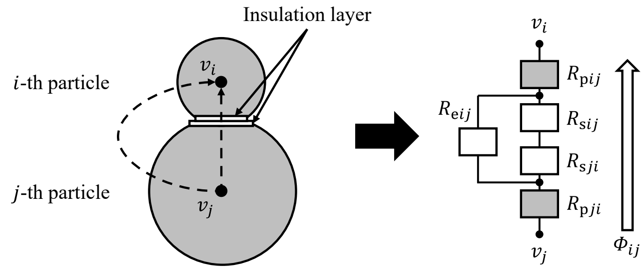

Fig. 4. Particles in contact and magnetic circuit between them.

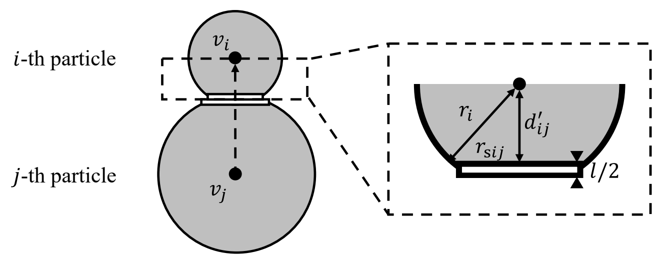

Fig. 5. Dimensions for magnetic reluctances for particles in contact.

III. Magnetic Circuit Method

This section introduces the magnetic circuit method based on the SMC model mentioned above. We formulate the flux and magnetic reluctances between two particles. Then, we derive the magnetic circuit equation to analyze the macroscopic properties of SMC. Finally, we describe identification of the microscopic properties of the SMC particles which are necessary for the macroscopic analysis.

A. Magnetic Circuit between Two Particles

Fig. 4 illustrates the particles that contact through the insulation layers and the magnetic circuit between them. In the magnetic circuit method, the magnetic scalar potential v_i is assigned at the center of i-th particle as the unknown variable. The magnetic flux between i-th and j-th particles, Φ_{ij}, is determined from

$$\Phi_{ij} = \frac{v_i - v_j}{R_{ij}}, \tag{3}$$

where R_{ij} denotes the magnetic reluctance between i-th and j-th particles. This is composed of the reluctance of i-th particle facing j-th particle, $R_{\mathrm{p}ij}$, the reluctance of the insulation layer on the contact surface of i-th particle facing j-th particle, $R_{\mathrm{s}ij}$, and vice versa, $R_{\mathrm{p}ji}$ and $R_{\mathrm{s}ji}$. In addition, the magnetic reluctance $R_{\mathrm{e}ij}$ is defined for the flux path beside the contact surface. As a result, R_{ij} for the particles in contact would be written as

$$R_{ij} = R_{\mathrm{p}ij} + \frac{1}{\dfrac{1}{R_{\mathrm{s}ij} + R_{\mathrm{s}ji}} + \dfrac{1}{R_{\mathrm{e}ij}}} + R_{\mathrm{p}ji}. \tag{4}$$

In this study, the reluctance $R_{\mathrm{p}ij}$ is attributed to a half of the particle cut out at the contact surface, and $R_{\mathrm{s}ij}$ is attributed to a cylinder with height $l/2$ and radius equal to that of the contact surface, $r_{\mathrm{s}ij}$, as shown in Fig. 5. Note that $r_{\mathrm{s}ij}$ is evaluated based on the model obtained by DEM for each pair of contacted particles, which share the common overlapping region. In our experience with DEM, neighboring particles either do not overlap completely or have overlapping regions. It would be difficult for all the particles in contact, resulting from DEM, to have point contact. The magnetic reluctances are expressed as follows:

$$\begin{aligned} R_{\mathrm{p}ij} &= \frac{1}{\mu_i}\int_0^{d'_{ij}} \frac{dx}{S_i(x)} \\ &= \frac{1}{\mu_i}\frac{1}{2\pi r_i}\ln\frac{r_i + d'_{ij}}{r_i - d'_{ij}}, \end{aligned} \tag{5a}$$

$$\begin{aligned} R_{\mathrm{s}ij} &= \frac{1}{\mu_0}\frac{l/2}{\pi r_{\mathrm{s}ij}^2} \\ &= \frac{1}{\mu_0}\frac{l/2}{\pi\left(r_i^2 - {d'_{ij}}^2\right)}, \end{aligned} \tag{5b}$$

where $S_i(x), d'_{ij}$ denote the cross-sectional area of i-th particle at the distance x from the center of the particle and the distance from the center of the particle to the contact surface (thus, $R_{\mathrm{p}ij} \neq R_{\mathrm{p}ji}$ and $R_{\mathrm{s}ij} \neq R_{\mathrm{s}ji}$), and μ_0, μ_i, l denote the permeabilities of vacuum and i-th particle, and insulation layer thickness, respectively. For static analysis, $\mu_i = \mu_{\mathrm{r}}\mu_0$ (μ_{r} is the relative permeability of the particles). In the frequency domain analysis to evaluate eddy current loss, it is assumed that

$$\mu_i = \mu_{\mathrm{r}}\frac{2(1 - \tan z_i / z_i)}{(1 - z_i^2)\tan z_i / z_i - 1}, \tag{6a}$$

$$z_i = r_i\sqrt{-j\omega\mu_{\mathrm{r}}\mu_0\sigma}, \tag{6b}$$

where ω, σ denote angular frequency and the electrical conductivity of the particle. Equations (6a) and (6b) represents the complex permeability of a single sphere [6], [14]. In addition, $R_{\mathrm{e}ij}$ is evaluated assuming that the shaded area shown in Fig. 6 is a vacuum (thus, $R_{\mathrm{e}ij} = R_{\mathrm{e}ji}$), as follows:

$$\begin{aligned} R_{\mathrm{e}ij} &= \frac{1}{\mu_0}\frac{D_{ij}}{\left(\pi r_j^2 - \pi r_{\mathrm{s}ji}^2\right)} \\ &= \frac{1}{\mu_0}\frac{D_{ij}}{\left(\pi r_j^2 - \pi\left(r_j^2 - {d'_{ji}}^2\right)\right)} \\ &= \frac{1}{\mu_0}\frac{D_{ij}}{\pi {d'_{ji}}^2}. \quad \left(r_i \leq r_j\right) \end{aligned} \tag{7}$$

On the other hand, flux can pass through particles that are not in contact but are close enough to each other. Between such particles, we introduce magnetic circuit composed only of a cylinder with height $D_{ij} - \left(r_i + r_j\right)$ radius αr_i ($r_i \leq r_j$ and $\alpha \leq 1$) and ignore the magnetic reluctance inside the particles, as shown in Fig. 7. This reluctance R_{ij} is evaluated by

$$R_{ij} = \frac{1}{\mu_0}\frac{D_{ij} - \left(r_i + r_j\right)}{\pi(\alpha r_i)^2}. \quad \left(r_i \leq r_j\right) \tag{8}$$

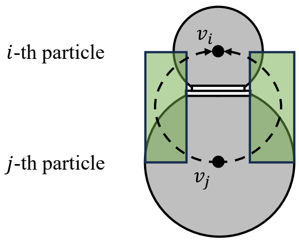

Fig. 6. Flux path beside contact surface.

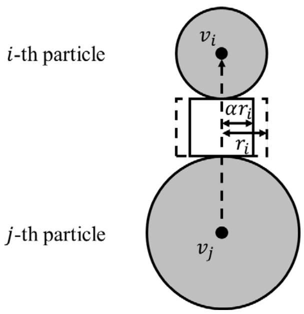

Fig. 7. Flux path between particles not in contact.

The effective radius factor α is introduced because the flux is not expected to propagate outside the cylinder whose radius is greater than r_i. In this study, we set $\alpha = 0.8$ so that the computed macroscopic permeability is close to the observed value. This magnetic circuit is considered only for the particles which are not in contact but fulfill the following condition:

$$D_{ij} \leq r_i + r_j + 2r_{\min}, \tag{9}$$

where $r_{\min}$ is the minimum radius in the distribution which is 1.5 μm in this work.

B. Magnetic Circuit Composed of Multiple Particles

Fig. 8 shows an iron particle surrounded by several particles. We observe this configuration in the image of the SMC cross section [4]. By applying Kirchhoff's circuit law to the magnetic flux, we have

$$\sum_j \Phi_{ij} = 0, \tag{10}$$

where j represents the particles in the vicinity of particle i. We can determine v_i from (3) and (10) with use of (4)-(9) by introducing the source term mentioned below.

C. Formulation of Magnetic Circuit Equation

Fig. 9 shows the entire structure of the magnetic circuit which corresponds to SMC immersed in uniform external magnetic field B_{ex} [2]. The magnetic circuit composed of N nodes (N particles) is connected to the constant flux source $\Phi_{\mathrm{ex}} = B_{\mathrm{ex}} S_{\mathrm{SMC}}$ via node 0 and node $N+1$, where S_{SMC} denotes the area of the upper and lower surfaces of the SMC model. The equations derived from Kirchhoff's circuit law for node 0 and node $N+1$ are

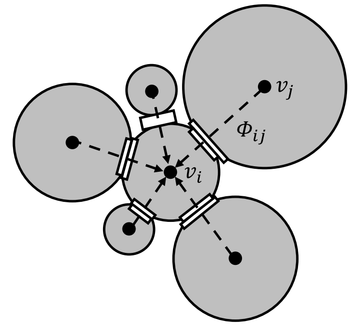

Fig. 8. Particle surrounded by multiple particles.

$$\sum_j \Phi_{0,j} = \Phi_{\mathrm{ex}}, \tag{11a}$$

$$\sum_j \Phi_{N+1,j} = -\Phi_{\mathrm{ex}}, \tag{11b}$$

where j represents the particles in contact to the upper and lower surfaces (mass plates). The magnetic circuit equation for all the particles can be expressed in matrix form

$$\mathrm{R}\boldsymbol{v} = \boldsymbol{\Phi}, \tag{12}$$

where $\mathrm{R} \in \mathbb{R}^{(N+2)\times(N+2)}$ is the reluctance matrix, $\boldsymbol{\Phi} = \{\Phi_i\}^T \in \mathbb{R}^{N+2}$ is the external flux vector (where $\Phi_i = 0$ for $i = 1, \dots, N$, $\Phi_0 = \Phi_{\mathrm{ex}}$, and $\Phi_{N+1} = -\Phi_{\mathrm{ex}}$), and $\boldsymbol{v} = \{v_i\}^T \in \mathbb{R}^{N+2}$ is the magnetic scalar potential vector. By solving (12), we finally obtain $\boldsymbol{v}$ by which we evaluate the macroscopic properties of the SMC model, as described in III. D.

Because the number of unknowns in the magnetic circuit is much smaller than in FEM, the former does not impose a large computational burden. Table III compares the number of elements required to represent model A2 in FEM and the magnetic circuit method, assuming grid meshing in FEM. In FEM, fine meshing is required to accurately represent thin insulation layer. As a result, the number of the elements can become quite large, especially for the large three-dimensional model, whereas the magnetic circuit method does not require such many elements since the insulation layer is modeled as the magnetic reluctances. Note that the computational burden of the

TABLE III
NUMBER OF REQUIRED ELEMENTS IN EACH METHOD

Method	Number of elements
FEM, grid mesh size = 0.1 μm	4.067×10^8
Magnetic circuit method	1184

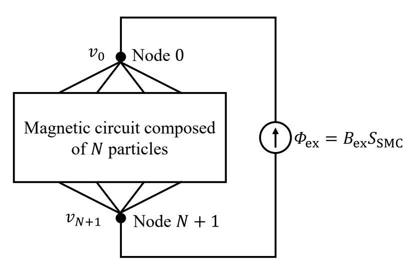

Fig. 9. Entire structure of magnetic circuit.

TABLE IV
OPTIMIZATION SETTINGS FOR MICROSCOPIC PARAMETER IDENTIFICATION

Name	Value
Number of initial data points $(-)$	10
Maximum step in optimization $(-)$	100
Acquisition function	Expected improvement
Strength of magnetic field B_{ex} (mT)	50
Sampling frequencies f_i (kHz)	$\{100, 200, \dots, 700\}$
Relative permeability μ_{r} of the particles	$\{1500, 2500, 3500\}$
Parameter range	$0.01\ \mu\mathrm{m} \le l \le 1.0\ \mu\mathrm{m}$ $1.0\times10^5\ \mathrm{S/m} \le \sigma \le 1.0\times10^7\ \mathrm{S/m}$

magnetic circuit method does not depend on the thickness of the insulation layer l, which is desirable especially when l is quite small compared to the size of the particles.

D. Evaluation of Macroscopic Permeability and Eddy Current Loss

The macroscopic relative permeability of SMC, $\langle\mu_{\mathrm{r}}\rangle$, is evaluated using the magnetomotive force $F = v_0 - v_{N+1}$ and the path length L (equals to the height of the SMC model in Fig. 3) as follows [2]:

$$\langle\mu_{\mathrm{r}}\rangle = \frac{B_{\mathrm{ex}}L}{\mu_0 F}. \tag{13}$$

The eddy current loss in particle i is evaluated using the complex permeability as follows [13]:

$$p_{\mathrm{e},i} = \frac{|\boldsymbol{B}|_i^2}{2}\mathrm{Re}\left(\frac{j\omega}{\mu_i^*}\right), \tag{14}$$

where $|\boldsymbol{B}|_i$ denotes the magnetic flux density of i-th particle and $*$ represents the complex conjugate. We determine $|\boldsymbol{B}|_i$ by considering the following different representations of magnetic energy density of i-th particle, $w_{\mathrm{M},i}$ and $w_{\mathrm{m},i}$

$$w_{\mathrm{M},i} = \frac{|\boldsymbol{B}|_i^2}{2\mu_i}, \tag{15a}$$

$$w_{\mathrm{m},i} = \frac{1}{2\mu_i}\sum_j\left(\frac{\Phi_{ij}}{\bar{S}_{ij}}\right)^2, \tag{15b}$$

where $\bar{S}_{ij}$ denotes the average cross-sectional area of the flux path of i-th particle facing j-th particle. By imposing the condition $w_{\mathrm{M},i} = w_{\mathrm{m},i}$, we obtain

$$|\boldsymbol{B}|_i = \sqrt{\sum_j\left(\frac{\Phi_{ij}}{\bar{S}_{ij}}\right)^2}. \tag{16}$$

The eddy current loss density of the whole SMC model, p_{e}, can be obtained by

$$p_{\mathrm{e}} = \frac{1}{V}\sum_{i=1}^{N} V_i p_{\mathrm{e},i}, \tag{17}$$

where V, V_i denotes the volume of the SMC model and i-th particle.

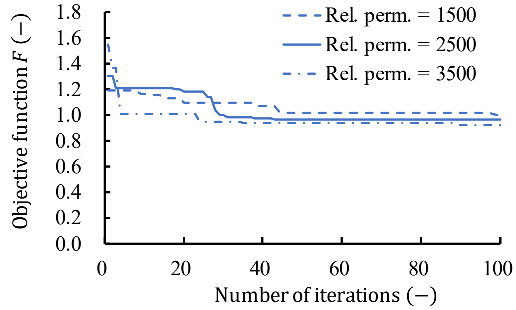

Fig. 10. Convergence history of optimizations. "Rel. perm." stands for Relative permeability.

E. Microscopic Parameter Identification

To calculate the macroscopic permeability and eddy current loss of SMC, we need to identify the microscopic properties $\mu_{\mathrm{r}}, l, \sigma$ which are difficult to measure directly. It became clear that μ_{r} does not have a significant effect on the macroscopic properties as long as it is large enough (say $\mu_{\mathrm{r}} > 1000$), according to the numerical results shown in section IV. A. Thus, we assume the relative permeability of the bulk iron for μ_{r}, and identify l and σ using Bayesian optimization [15].

The optimization problem is defined as follows.

$$\min. F(l,\sigma) = \frac{|\langle\mu_{\mathrm{r}}\rangle - \langle\mu_{\mathrm{r}}\rangle'|}{\langle\mu_{\mathrm{r}}\rangle'} + \sum_{f_i}\frac{|p_{\mathrm{e}} - p_{\mathrm{e}}'|}{p_{\mathrm{e}}'}, \tag{18}$$

where $\langle\mu_{\mathrm{r}}\rangle', p_{\mathrm{e}}'$ denote the measured values of the macroscopic permeability and eddy current loss of SMC, and f_i denotes the sampling frequencies for the eddy current loss evaluation. We would introduce a weighting coefficient on the second term of (18) to balance the effects of the first and second terms for larger numbers of sampling frequencies.

IV. NUMERICAL RESULTS

In this section the numerical results are reported. The result of microscopic parameter identification using model A2 is presented. Then, the identified parameters are applied to the analysis of the macroscopic properties of models A1 and A3.

A. Microscopic Parameter Identification Using Model A2

Microscopic parameter identification was conducted by solving optimization problem (18) using Bayesian optimization method. The optimization setting is summarized in Table IV. In the simulation, μ_{r} was assumed to be $\{1500, 2500, 3500\}$ with reference to typical bulk iron permeability. We conducted three runs of optimizations changing μ_{r}.

Fig. 10 shows the convergence history of three optimizations with different μ_{r}. As can be seen, the best values of the objective function F hardly change by μ_{r}. Table V shows the identified microscopic parameters by the optimizations.

Figs. 11 and 12 show the macroscopic permeability $\langle\mu_{\mathrm{r}}\rangle$ and the eddy current loss p_{e} calculated using the identified microscopic parameters. For different values of μ_{r}, the calculated macroscopic properties agreed well with the measured results.

TABLE V
IDENTIFIED MICROSCOPIC PARAMETERS USING A2 MODEL

Assumed value of μ_r $(-)$	l (μm)	σ (S/m)
1500	0.160	4.95×10^6
2500	0.161	4.96×10^6
3500	0.162	5.38×10^6

Fig. 13 shows $|\boldsymbol{B}|_i$ for all the particles. It can be seen that flux passes mainly through large particles from top to bottom. This tendency is consistent to the results obtained by FEM [3], [9] where the magnetic flux tends to concentrate in the paths with low magnetic reluctance, which contain few insulating layers due to many large particles.

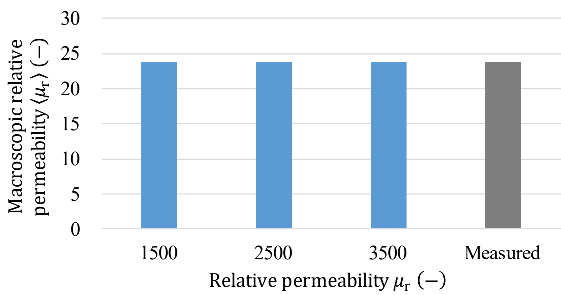

Fig. 11. Macroscopic permeability of model A2 calculated by magnetic circuit method using the identified parameters.

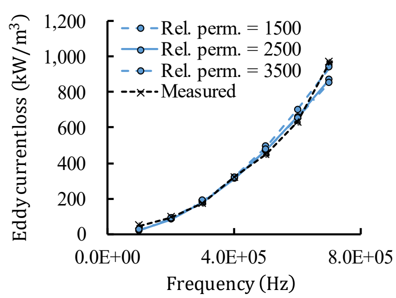

Fig. 12. Eddy current loss of model A2 calculated by magnetic circuit method using the identified parameters. "Rel. perm." stands for relative permeability.

B. Validation of Identified Microscopic Parameters Using Models A1 and A3

We now apply the identified microscopic parameters to the analysis of the macroscopic properties of models A1 and A3. Hereafter, the identified parameters when $\mu_r = 2500$ in Table V are used for computation since no considerable difference exists among different μ_r. For model A1, $f_i = \{100, 200, \dots, 600\}$ (kHz), while for model A3, $f_i = \{100, 200, \dots, 800\}$ (kHz) for measurement reasons.

Figs. 14 and 15 shows the macroscopic permeability $\langle \mu_r \rangle$ and eddy current loss p_e for models A1 and A3. For model A1, $\langle \mu_r \rangle$ agreed with the measured result well, whereas small discrepancies were observed in p_e^{SMC}. For model A3, the magnetic circuit method overestimates $\langle \mu_r \rangle$. On the other hand, p_e is in better agreement with the measured result compared to model A1. From these results, it can be said that the identified microscopic parameters can be used in common across different

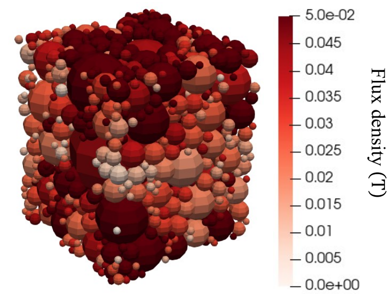

Fig. 13. Flux density distribution of A2 model calculated by magnetic circuit method using the identified parameters ($\mu_r = 2500$).

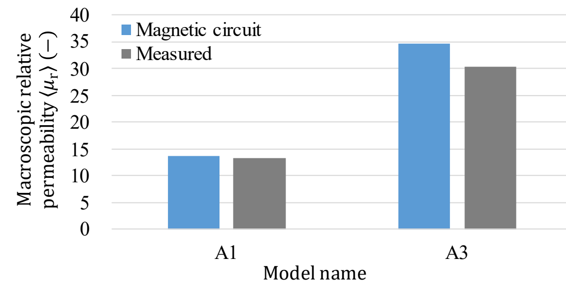

Fig. 14. Macroscopic permeability of models A1 and A3 computed by magnetic circuit method using the identified parameters ($\mu_r = 2500$).

models with the same particles but different filling rates, although we have to accept the small discrepancies.

Fig. 16 shows $|\boldsymbol{B}|_i$ for all the particles. In model A1 with a smaller filling rate, $|\boldsymbol{B}|_i$ tends to be large due to the fact that there are iron particles with relatively smaller number of particles in their vicinity, and flux would be concentrated among such particles, resulting in an overestimation of p_e. The opposite trend was observed in model A3, where many of particles are in close and there would be many flux paths which enhance $\langle \mu_r \rangle$.

V. CONCLUSION

In this paper, we have proposed a magnetic circuit method based on DEM. In this method, the magnetic circuit is constructed from the DEM model. Microscopic parameter of SMC particles is identified, and they are used for evaluation of the macroscopic permeability and eddy current loss of SMC with different filling rates. The computed results are consistent with the measured results.

In the future, we plan to extend the proposed method for nonlinear analysis to consider the magnetic saturation in SMC particles. In addition, we plan to optimize the particle distribution and material properties on the basis of the proposed method to maximize the macroscopic permeability and minimize the losses.

ACKNOWLEDGMENT

This work was supported partly by JSPS Research Fellowships for Young Scientists 23KJ0013.

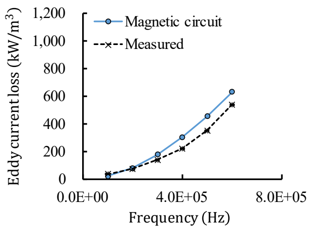

(a) A1 model

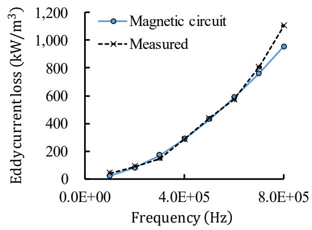

(b) A3 model

Fig. 15. Eddy current loss of models A1 and A3 computed by magnetic circuit method using the identified parameters ($\mu_{\mathrm{r}} = 2500$).

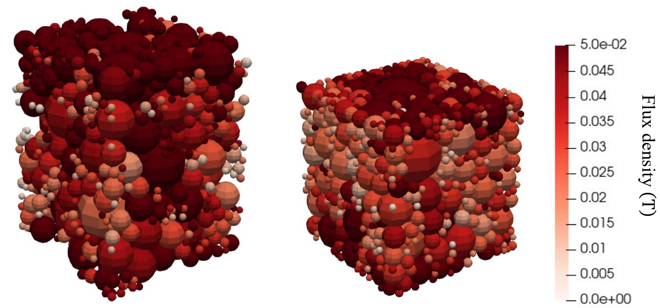

(a) A1 model (b) A3 model

Fig. 16. Flux density distribution of models A1 and A3 calculated by magnetic circuit method using the identified parameters ($\mu_{\mathrm{r}} = 2500$).

References

[1] F. Ollendorff, "Magnetostatik der massekerne," *Arch. f. Eledtrotechnik.*, vol. 25, pp. 436-447, 1931.

[2] Y. Ito, H. Igarashi, M. Suzuki, Y. Iwasaki, and K. Kawano, "Effect of Magnetic Contact on Macroscopic Permeability of Soft Magnetic Composite," *IEEE Trans. Magn.*, vol. 52, no. 3, pp. 1-4, Art no. 9400804, 2016.

[3] A. Maruo and H. Igarashi, "Analysis of Magnetic Properties of Soft Magnetic Composite Using Discrete Element Method," *IEEE Trans. Magn.*, vol. 55, no. 6, pp. 1-5, Art no. 2002205, 2019.

[4] H. Waki, H. Igarashi, and T. Honma, "Estimation of effective permeability of magnetic composite materials," *IEEE Trans. Magn.*, vol. 41, no. 5, pp. 1520-1523, 2005.

[5] Y. Ito and H. Igarashi, "Computation of Macroscopic Electromagnetic Properties of Soft Magnetic Composite," *IEEE Trans. Magn.*, vol. 49, no. 5, pp. 1953-1956, 2013.

[6] Y. Sato and H. Igarashi, "Time-Domain Analysis of Soft Magnetic Composite Using Equivalent Circuit Obtained via Homogenization," *IEEE Trans. Magn.*, vol. 53, no. 6, pp. 1-4, Art no. 7402204, 2017.

[7] P. A. Cundall and O. D. L. Strack, "A discrete numerical model for granular assemblies," *Géotechnique*, vol. 29, no. 1, pp. 47-65, 1979.

[8] R. Balevičius, A. Džiugys, R. Kačianauskas, A. Maknickas, and K. Vislavičius, "Investigation of performance of programming approaches and languages used for numerical simulation of granular material by the discrete element method," *Computer Physics Communications*, vol. 175, no. 6, pp. 404-415, 2006.

[9] H. Sato, A. Maruo, and H. Igarashi, "Analysis of nonlinear magnetic properties of soft magnetic composite using 2D and 3D discrete element methods," *IJAEM*, vol. 64, no. 1-4, pp. 483-492, 2020.

[10] H. Sato and H. Igarashi, "3-D Analysis of Soft Magnetic Composite Using Discrete Element Method in Frequency Domain," *IEEE Trans. Magn.*, vol. 57, no. 6, pp. 1-4, Art no. 2000504, 2021.

[11] J. Vesa and P. Rasilo, "Producing 3-D Imitations of Soft Magnetic Composite Material Geometries," *IEEE Trans. Magn.*, vol. 55, no. 10, pp. 1-10, Art no. 2002510, 2019.

[12] J. Vesa and P. Rasilo, "Comparison of 3-D and 2-D models of a soft magnetic composite material," *J. Magn. Magn. Mater.*, vol. 536, 2021.

[13] H. Igarashi, "Semi-Analytical Approach for Finite-Element Analysis of Multi-Turn Coil Considering Skin and Proximity Effects," *IEEE Trans. Magn.*, vol. 53, no. 1, pp. 1-7, Art no. 7400107, 2017.

[14] A. Berthault, D. Rousselle, and G. Zerah, "Magnetic properties of Permalloy microparticles," *J. Magn. Magn. Mater.*, vol. 112, nos. 1–3, pp. 477-480, 1992.

[15] H. Igarashi, Topology optimization and AI-based design of power electronic and electric devices, Academic Press, 2024.